COMMUNICATIONS PHYSICS

ARTICLE

Check for updates

https://doi.org/10.1038/s42005-020-0357-8 OPEN

Asymmetric Fermi velocity induced chiral magnetotransport anisotropy in the type-II Dirac semi-metal $PtSe_2$

Jian Sun[1✉], Russell S. Deacon[2,3], Wenchen Luo[1], Yahua Yuan[1], Xiaochi Liu[1], Haipeng Xie[1], Yongli Gao[1,4] & Koji Ishibashi[2,3]

$PtSe_2$ is a recently discovered type-II Dirac semi-metal with heavily tilted Dirac cone in *z*-direction of the momentum. Negative magnetoresistance (MR) is expected as a signature of the chiral anomaly in the *x*–*y* plane where Lorentz invariance is maintained. Here we report the observation of negative MR in $PtSe_2$ thin flakes with magnetic fields aligned parallel to the current path and crystal *a*-axis. Systematic measurements reveal that this phenomenon is field-vector and temperature sensitive, thereby confirming chiral anomaly as its origin. Furthermore, the chiral anomaly is tunable with an electric field. Interestingly, negative MR vanishes along the orientation *a*′ perpendicular to *a*-axis. This clear anisotropy is ascribed to the anisotropic distribution of the Fermi velocity. A weaker chiral anomaly is caused in *a*′ and therefore masked by the trivial background signal. Our results highlight the importance of even a small material anisotropy when studying the chiral magnetotransport of Weyl/Dirac semi-metals.

[1] School of Physics and Electronics, Central South University, 932 South Lushan Road, Changsha 410083, China. [2] Advanced Device Laboratory, RIKEN, 2-1 Hirosawa, Wako, Saitama 351-0198, Japan. [3] Center for Emergent Matter Science (CEMS), RIKEN, 2-1 Hirosawa, Wako, Saitama 351-0198, Japan. [4] Department of Physics and Astronomy, University of Rochester, Rochester, NY 14627, USA. ✉email: jian.sun@csu.edu.cn

Weyl semi-metals, which host emergent quasiparticles known as Weyl fermions, have recently drawn broad interest in condensed matter physics[1–4]. In a Weyl semi-metal, the conduction and valence bands exhibit a linear dispersion at pairs of isolated Weyl points for all lattice momentum vectors, leading to Fermi arcs residing in the surface states at different Weyl points carrying opposite chirality. Three-dimensional Dirac semi-metals have a very close relationship with Weyl semi-metals. One Dirac cone can be considered as two superimposed Weyl cones with opposite chirality[5–7]. Applying a magnetic field breaks the time reversal symmetry, therefore leading to the evolution of one Dirac cone into two Weyl nodes. Most Weyl and Dirac semi-metals have been discovered experimentally by directly examining the existence of Weyl/Dirac nodes and Fermi arcs in their energy band structures via angle-resolved photoemission spectroscopy (ARPES)[2,3,8,9].

Type-II Weyl and Dirac semi-metals are a newly proposed and discovered material with an open Fermi surface in contrast with the closed point-like Fermi surface in the conventional type-I Weyl and Dirac semi-metals[10–12]. The energy spectrum consists of strongly tilted Dirac Cones along certain momentum directions in contrast to a straightly standing type-I Dirac cone (Fig. 1a, b). The cross section of the Fermi surface resembles a pair of pockets. The tilted angle is so large that it appears that the Lorentz invariance is broken. The energy spectrum has already been verified by a series of ARPES experiments[13–18].

In magnetotransport, the presence of Weyl nodes can be seen, when an external magnetic field B is applied along the transport direction of current I, i.e., $B \parallel I$. Under such conditions, electrons can be pumped from one Weyl node to the other through their band structure connection, leading to an out-of-equilibrium distribution of charges between the Weyl nodes enhancing the conductance[19]. The change of conductivity can be estimated using

$$\Delta\sigma = \frac{e^4 B^2 \tau v_{\mathrm{F}}^3}{4\pi^2 \hbar \Delta E^2}, \qquad (1)$$

where τ is the inter-node relaxation time, v_{F} is the Fermi velocity, and ΔE is the energy difference between Fermi surface and Dirac point[20]. In the steady state, the charge pumping is relaxed through inter-node scattering. Hence, this chiral negative magnetoresistance (MR) is often considered as a transport signature for the non-ferromagnetic Dirac and Weyl semi-metals[21–23]. However, one must be very careful when drawing this conclusion as other effects can lead to negative MR in systems with no chirality. For instance, a geometric effect, so-called current jetting, is able to cause negative MR in the semi-metals having high carrier mobility even without well-defined chirality[24–26]. Moreover, in a topological insulator, a temperature insensitive negative MR has been observed and discussed as a result of anomalous velocity and orbital moment induced by Berry curvature, in which the chiral anomaly is not necessary[27]. In addition, ΔE can be controlled by applying an electric field, giving the possibility to electrically tune the chiral anomaly[28].

The breaking of Lorentz invariance in the type-II Weyl/Dirac semi-metal gives rise to anisotropic chiral MR, i.e., vanishing negative MR along the titling axis of the Dirac cones, as in this geometry the pumping of carriers is quenched. Such magnetotransport anisotropy has been considered as a solid experimental evidence of the broken Lorentz invariance. It has been verified in the type-II Weyl semi-metal WTe_2, which has tilted Dirac cones in its basal plane[29,30]. $PtSe_2$ is a new type-II Dirac semi-metal recently verified by ARPES[17,31]. It has a Dirac cone tilted along z axis, therefore leaving the Lorentz invariance preserved in the x–y plane. As this material has been only recently explored, only a weak chiral negative MR of $\sim -0.1\%$ has been reported recently[32]. The in-depth transport measurements are still lacking[33]. As a transition metal dichalcogenide of $1T$ structural phase, $PtSe_2$ hosts a nonnegligible in-plane anisotropy, which may have an important role in its magnetotranport in addition to the chiral anomaly. Hence, it is of great interest to investigate the MR anisotropy in $PtSe_2$.

In this paper, we report a study of magnetotransport in thin flakes of the type-II Dirac semi-metal $PtSe_2$. Measurements reveal clear negative longitudinal MR when the electric and magnetic fields are parallel. Moreover, the negative MR is found to be angle (between B and I) and temperature sensitive, being significantly suppressed by misaligning current and magnetic field or rising the temperature, both signatures of the chiral anomaly. We further demonstrate that by applying an external electric field using a gate these unique chiral transport properties can be electrically

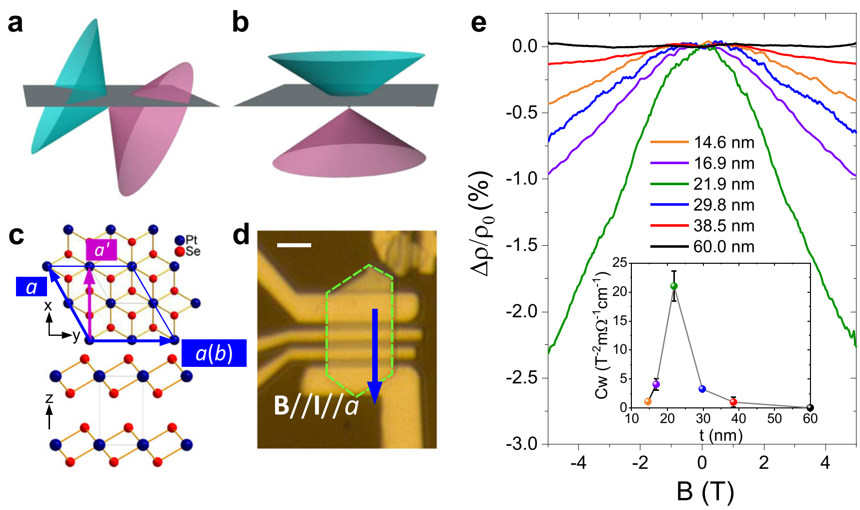

Fig. 1 Crystal structure and the negative magnetoresistance. **a**, **b** Schematic drawings of a tilted type-II Dirac cone and a type-I Dirac cone, respectively. **c** Crystal structure of the type-II Dirac semi-metal $PtSe_2$. The solid blue arrows present two equivalent $a(b)$ axes. The purple arrow shows an axis a' defined in normal to a. **d** Microscopic photo of a typical fabricated $PtSe_2$ device with four-contact geometry. The dashed line highlights the sharp edges of the flake intersecting with an angle of 120°. Current and magnetic field are applied in parallel along the a axis indicated by the blue arrow. Scale bar: 2 µm. **e** Negative magnetoresistance $\Delta\rho/\rho_0$ measured in the $PtSe_2$ flakes with various thicknesses. Inset: Extracted chiral anomaly coefficient C_{w} with respect to the sample thickness. The error bars are the standard deviation and in some cases are smaller than the data point.

controlled. More interestingly, without breaking the Lorentz invariance in the x–y plane, negative MR vanishes in the direction perpendicular to the in-plane crystal axis, which we attribute as arising from a slightly anisotropic distribution of Fermi velocity.

Results

Anisotropic crystalline and device preparation. Bulk $PtSe_2$ possesses a $1T$ structural phase, which crystallizes in the centrosymmetric CdI_2-type structure with the space group of $P\bar{3}m1$ (Fig. 1c). The structure can be regarded as hexagonal close-packed Se atoms where Pt atoms occupy the octahedral sites in alternative Se layers. Two equivalent crystal axes, a and b, are defined with an angle of 60° or 120° as depicted in Fig. 1c. The adjacent unoccupied Se layers are held together by weak van der Waals interactions. Theoretical calculations and ARPES show that the Fermi surface in $PtSe_2$ sits at >1 eV above the Dirac point[17,33]. The large ΔE hinders the detection of the chiral anomaly induced negative MR in the stoichiometric $PtSe_2$. X-ray photoemission spectroscopy measurement reveals a Pt:Se composition ratio of 1 : 2.08 for the crystal used in this work (Methods and Supplementary Fig. 1). In this Se-rich crystal, the Fermi energy could be moved massively towards the Dirac point, therefore leading to the enhanced negative MR. A similar strategy has been demonstrated for tuning ΔE in a type-II Weyl semi-metal $WTe_{1.98}$[29].

Mechanically exfoliated thin $PtSe_2$ flakes are used for the magnetoresistance measurements. Sharp facet-like edges with edge angles of 60° or 120° are noted in majority of the exfoliated flakes, as shown in Fig. 1d. It can be interpreted therefore that $PtSe_2$ has the most strongly bonded orientations along the $a(b)$ axis. As a result, the cleaved edges are preferable along the $a(b)$ axis, making it feasible to determine the crystal orientation of the flakes. The same strategy has been employed to determine the crystal axis in the $1T'$ phase ReS_2[34]. To fabricate the devices, we select only those flakes showing sharp facet-like edges with angles of 60° or 120°. Figure 1d shows the optical image of a typical device, where the contacts are aligned perpendicularly to the long edge, leading to the electric field E, i.e. current I, along the a axis. Hall measurements show a mobility of ~520 $cm^2 V^{-1} s^{-1}$ for $PtSe_2$ (Supplementary Fig. 2). Considering such a low mobility current jetting is very unlikely to occur. Nevertheless, contacts fully covering the flake were employed to completely avoid the geometric current jetting effect[25,26].

Negative magnetoresistance. We first examine negative MR along the a axis. The longitudinal MR is measured in the $PtSe_2$ flakes at magnetic fields $B \parallel I \parallel a$. Figure 1e plots the MR data in the flakes with varied thickness t. Note the metal-to-semiconductor transition may occur in $PtSe_2$ as its thickness is reduced[35]. We confirm that the thin flakes still preserve metallic behavior by the monotonic decrease of resistivity measured with reducing temperature (Supplementary Fig. 3). In a bulk-like flake of 60-nm-thickness only the trivial positive MR is observed. The pronounced negative MR starts to appear and is enhanced with decreasing t. A maximum negative MR of $\sim -2.25\%$ is measured in the sample with $t = 21.9$ nm at $5T$. As the measured flakes become thinner the magnetotransport in the bulk transits from three-dimensional to quasi-two-dimensional. Considering an ideal two-dimensional system, the in-plane magnetic field should not introduce any trivial positive MR. As a result, the positive MR signal can be significantly suppressed in thin flakes, therefore making the measurement of chiral negative MR feasible. Similar phenomenon has been observed in the Weyl semi-metal WTe_2[28]. In contrast to the study on WTe_2, we observe that negative MR is weakened in flakes thinner than 20 nm. A possible scenario is ascribed to the doping from surface defects in the substrate. During our experiment, the substrate is inevitably subjected to plasma cleaning treatment and temperature cycles, which causes oxygen deficiency defects and dangling bonds in SiO_2[36]. Consequently electron accumulation at the $PtSe_2$–SiO_2 interface may be sufficient to push the Fermi energy away from the Dirac point in a thin $PtSe_2$ flake, causing the observed decease in negative MR according to Eq. (1). Overall, due to the relatively large ΔE, the values of MR ratios observed in our experiments are about one to two orders of magnitude lower compared to those systems with high mobility and low ΔE, such as Na_3Bi ($\sim -80\%$)[21], GdPtBi ($\sim -75\%$)[26], Cd_3As_2 ($\sim -65\%$)[23], and doped WTe_2 ($\sim -40\%$)[29].

In the semi-classical limit, the strength of the chiral anomaly can be extracted quantitatively as the chiral coefficient C_W, by fitting the low-field negative MR data to the equation[22]

$$\Delta\sigma = C_W B^2 + C_{WAL}\frac{\sqrt{B}B^2}{B^2 + B_c^2} + C_{WL}\frac{B_c^2 B^2}{B^2 + B_c^2}, \qquad (2)$$

where C_{WAL} and C_{WL} are the weak anti-localization and weak localization coefficients, respectively, and B_C denotes the crossover field. The measured resistance changes in low magnetic fields mainly obey a parabolic law, excluding weak localization from the possible origins for this negative MR. The inset of Fig. 1e plots the evolution of C_W extracted from the low-field MR data within $2T$ with respect to the sample thickness.

Verification of chiral anomaly. To verify that the measured negative MR originates from the chiral anomaly, we first verify the angular-sensitivity of MR with misalignment between B and I. The current I is applied along the a axis during the measurements, while B is tilted away from I by an angle of θ (see inset of Fig. 2a). The MR remains negative within $\theta < 11°$ and increases to positive 10% at $B \perp I$ (Fig. 2a, b). The negative MR in $PtSe_2$ is known to be temperature sensitive in the case of a chiral anomaly. On the contrary, Berry curvature induced negative MR is temperature insensitive and can be maintained at high temperatures[27]. Figure 2c shows the temperature dependence of MR measured at $B \parallel I \parallel a$. It is clear that the negative MR is suppressed with increasing temperature; and it fully vanishes at 6K. On the basis of these findings, we rule out Berry curvature as the dominant mechanism for the observed negative MR. At higher temperatures the inter-node relaxation time of electrons decreases. Using Eq. (1), we semi-quantitatively estimate the change of τ with temperature as shown in Fig. 2d. Normalized τ rapidly decreases to zero at temperatures above 6 K where the inter-node relaxation is much faster than the charge pumping. At such temperatures charge pumping is impossible, therefore suppressing the chiral anomaly feature[37].

Electrical tuning of the chiral magnetotransport. Next, we demonstrate the electrical tuning of the chiral anomaly. Owing to its high conductivity (~10^6 S m^{-1}) and strong screening, the electrical tuning of the Fermi level of semi-metallic $PtSe_2$ is extremely challenging in its bulk form. Using a thin flake of ~10 nm-thickness, offers us the possibility to tune the Fermi energy in a small range by applying gate voltage. Here, the heavily doped silicon substrate is employed as a gate with the 300-nm-thick SiO_2 as dielectric layer. Figure 3 shows the MR measured at $B \parallel I \parallel a$ with various back gate voltages V_g from −30 to 30 V. The negative MR is mildly enhanced by a negatively increased V_g. This tendency can be more clearly read from the extracted C_W–V_g curve, which presents a tuning of 30% for C_W within the applied voltage range. According to Eq. (1), the negative MR is enhanced when the Fermi energy is moved towards the Dirac point. In order to tune the Fermi energy crossing the Dirac point, a thin high-κ dielectric layer or ionic gate would likely be required.

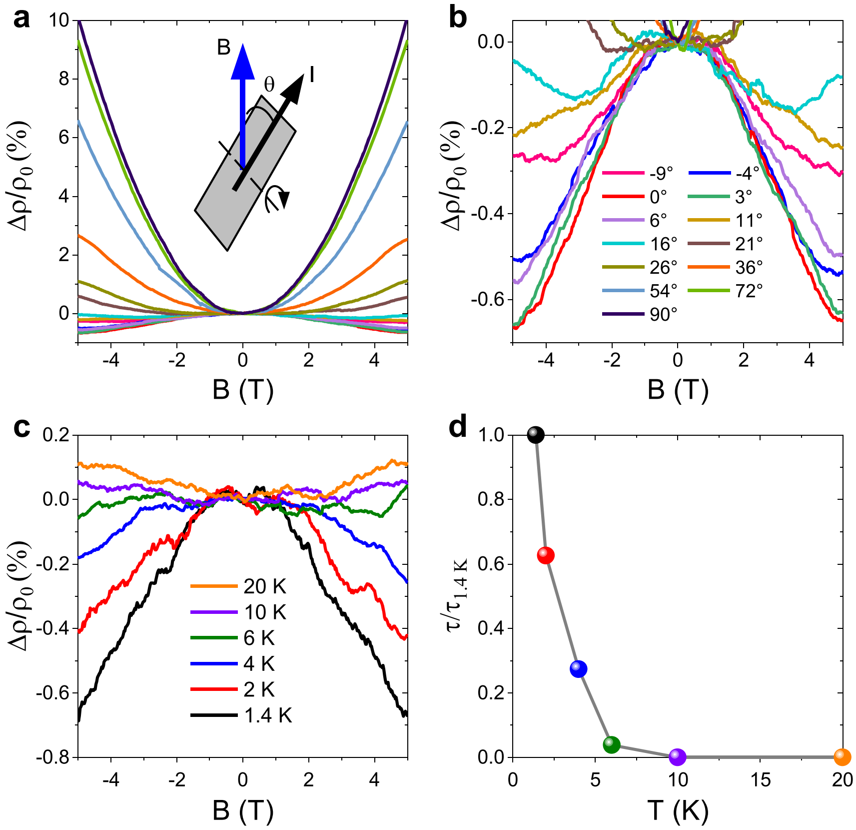

Fig. 2 Angular and temperature dependences of the negative magnetoresistance. **a** Angular dependence of the magnetoresistance $\Delta\rho/\rho_0$ measured in a $PtSe_2$ sample with the current $I \parallel a$ ($t = 29.8$ nm) at tilted magnetic field B. Inset: Schematic showing the rotation of a sample by the angle of θ in B, where the rotation axis is perpendicular to the current. **b** Zoomed-in details of the negative magnetoresistance regime in **a**. **c** Magnetoresistance measured in a $PtSe_2$ sample with $B \parallel I \parallel a$ ($t = 29.8$ nm) at varied temperatures. **d** Inter-node relaxation time τ normalized with the value measured at $T = 1.4$ K, extracted from **c**. The error bars are much smaller than the data point and are not presented.

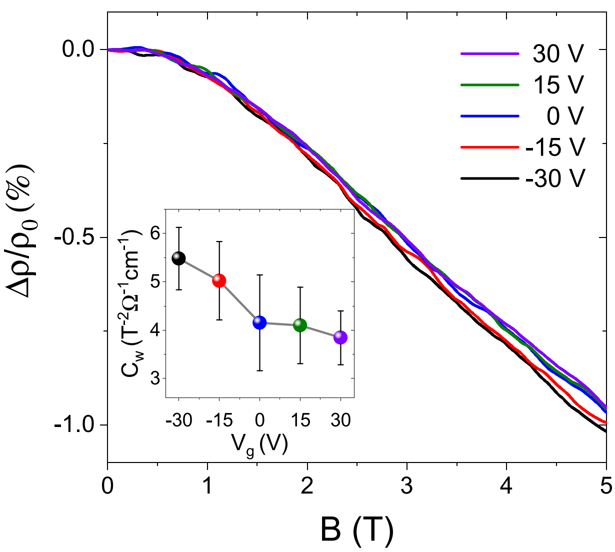

Fig. 3 Gate tunable negative magnetoresistance. Magnetoresistance $\Delta\rho/\rho_0$ measured with both magnetic field B and current I aligned to a axis, $B \parallel I \parallel a$ (flake $t = 16.9$ nm). Inset: The extracted chiral anomaly coefficient C_w at varied gate voltages. The error bars are the standard deviation.

Anisotropic chiral anomaly. As the Lorentz invariance holds in the x–y plane, no vanishing MR is predicted in $PtSe_2$ flakes despite the presence of a tilted Dirac cone. However, a notable in-plane anisotropy for $PtSe_2$, i.e., a deformed Dirac cone with the angle in its basal plane, has been seen in ARPES data[17]. Hence, it is of great interest to investigate whether any anisotropy of MR appears in the thin $PtSe_2$ flakes. We perform measurements of longitudinal MR at $B \parallel I$ along two distinct axes with the greatest difference in properties, i.e., a and $a' \perp a$ (Fig. 1c). The devices used are made from the same 29.8-nm-thick flake with current paths designed along a and a', respectively (inset of Fig. 4a). Surprisingly, at $B \parallel I \parallel a'$ positive MR is observed instead of a chiral negative MR (Fig. 4a). In contrast, along the a axis a negative MR is again measured as a signature of the chiral anomaly. Moreover, even at zero magnetic field the transport anisotropy indicates a four times greater resistivity along a' than that in a as plotted in Fig. 4b.

The vanishing of the chiral negative MR along a' can be attributed to an anisotropic distribution of Fermi velocity in-plane. The Hamiltonian near the Dirac point can be written as[38–40]

$$H = v_F(\alpha)\sigma \cdot \mathbf{p} + w p_z, \tag{3}$$

where $\sigma = (\sigma_x, \sigma_y, \sigma_z)$ with the Pauli matrices $\sigma_{x,y,z}$, and $\mathbf{p}$ is the three-dimensional momentum (p_x, p_y, p_z) with the azimuth α in the cylindrical polar coordinates. The tilt of the Dirac cone along the k_z direction is described by parameter w. The condition $|w/v_F| > 1$ breaks Lorentz invariance indicating that the material is a type-II Dirac semi-metal. The Fermi velocity $v_F(\alpha)$ may be a constant along the z axis but is not necessarily a constant in the x–y plane. As the Dirac cones are slightly deformed in the x–y plane in $PtSe_2$[17], the Hamiltonian does not have in-plane rotational symmetry. As there is only one Dirac cone in the Γ –

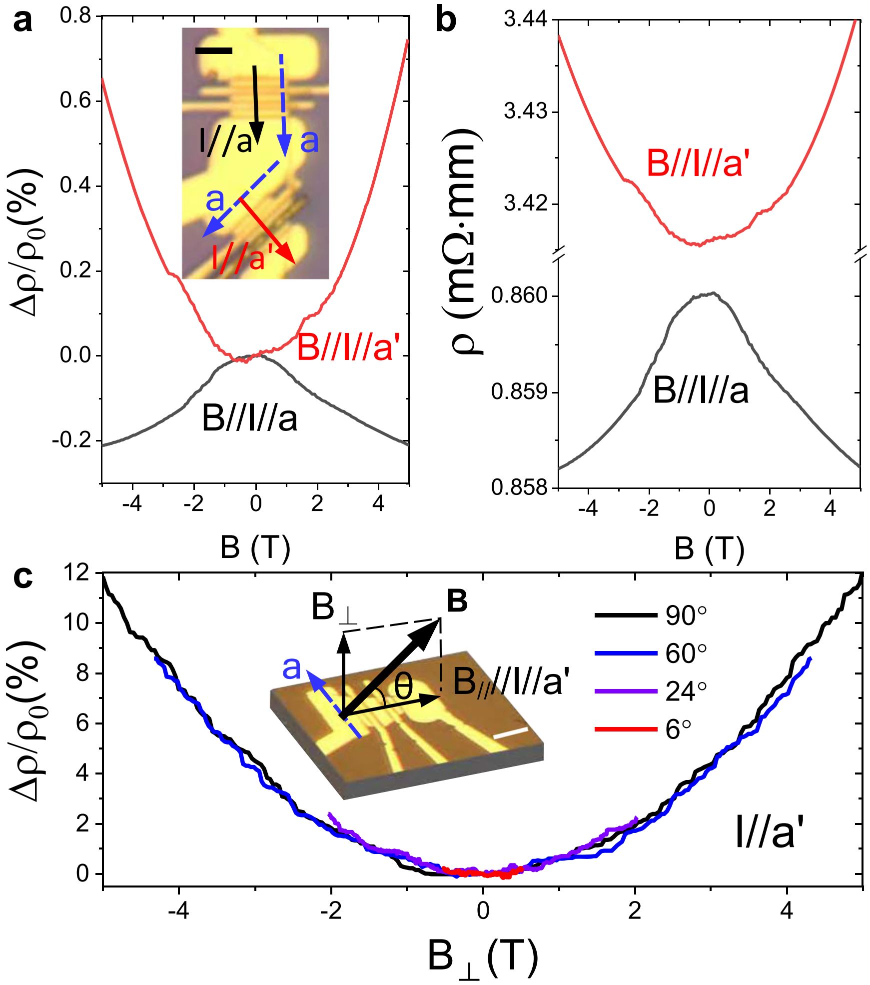

Fig. 4 Anisotropic magnetoresistance in $PtSe_2$. a Magnetoresistance $\Delta\rho/\rho_0$ measured in the $PtSe_2$ sample along a and a' ($t = 32$ nm). Inset: Microscopic photo of two devices made on the same flake with current $I \parallel a'$ (down) and $I \parallel a$ (up), respectively. Blue dashed arrows mark the orientations of a, solid arrows show the current direction. Scale bar: 2 μm. **b** Resistivity ρ corresponding to the magnetoresistance data plotted in **a**. **c** Angular dependence of the magnetoresistance measured in a $PtSe_2$ sample with $I \parallel a'$ ($t = 29.8$ nm). Inset: Microscopic photo of the measured device. The blue dashed arrow marks the orientations of a. The dark solid arrow shows the tilted magnetic field B misaligned from I by the angle of θ. Scale bar: 5 μm.

A line, the anisotropy of the cone directly affects the transport properties. The deformation of the Dirac cone can be translated into a Fermi velocity function $v_F(\alpha)$.

Experimentally, the Fermi velocity can be obtained from the dispersion of the energy bands of the system $v_F = \partial E/(\partial k\hbar)$. We need to know the local Fermi velocity at the Fermi surface, which corresponds to the transport properties by Eq. (1). Thus, we extract the dispersion relation of the data from ARPES measurement performed by Zhang et al.[17] to obtain a ratio of ~1.5 between the values of v_F in the a and a' directions, when the energy is ~10 meV above the Dirac point. We note that a slight change of v_F may significantly affect the magnetotransport properties of the system according to Eq. (1). where $\Delta\sigma \propto v_F^3$. It is straightforward that the measured conductivity signal $\Delta\sigma(a)/\Delta\sigma(a') \approx 3.4$. Considering a much higher resistivity in a', the negative MR due to the chiral anomaly is much weaker. As a result, the signature of the Chiral anomaly may be fully masked by the positive MR from the trivial bulk, even as the chirality in a' remains untouched.

Two-dimensionality in $PtSe_2$ flakes. Finally, we confirm the dimensionality of the trivial bulk for the thin $PtSe_2$ by measuring the angular dependence of MR with $I \parallel a'$. Noted that at $\theta = 0$, i.e., $B \parallel I \parallel a'$, no negative MR is anticipated. In Fig. 4c, MR curves are plotted as a function of the perpendicular component of tilted field $B_\perp$ at varied θ. These curves all collapse onto the same trace, which offers clear evidence of the quasi-two-dimensional nature for the thin flake. These results verify the aforementioned argument that in the thin flakes the trivial positive MR is significantly suppressed, making the detection of the weak chiral negative MR feasible. Furthermore, the application of the in-plane magnetic field in the measurement of chiral negative MR is not expected to discretize the energy bands of $PtSe_2$.

Discussion

In summary, we experimentally observe negative MR in thin flakes of the type-II Dirac semi-metal $PtSe_2$ along its crystal a axis. This unique magnetotransport phenomenon is found to be angle and temperature sensitive, verifying it as a consequence of the chiral anomaly. The chiral anomaly negative MR is demonstrated to be controllable by tuning the Fermi energy via the electric field. The negative MR vanishes along the a' axis even though the Lorentz invariance is still preserved in that orientation. We interpret this suppression as the consequence of an anisotropic distribution of Fermi velocity, which weakens the negative MR signal by one order. Our experiment indicates that an anisotropic chiral anomaly MR is not sufficient alone to support the existence of a tilted Dirac cone as the signature of a type-II Dirac semi-metal, especially for an anisotropic system.

Methods

Device fabrication and characterizations. Thin flakes with tens of nanometers thickness were mechanically exfoliated using tape from a bulk crystal (HQ Graphene) onto a p-doped silicon substrate covered with 300 nm thermal SiO_2. The thickness of flakes was measured by atomic force microscopy. The metal contacts for the 4-wire measurement were defined with titanium/palladium (0.5/80 nm) electrodes using e-beam lithograph and evaporation. Measurements were performed using standard lock-in techniques in a pumped He-4 refrigerator with a variable temperature insert. The sample was mounted on a single axis rotator with the alignment accuracy of sample orientation within 1°. Hall resistance was measured for the $PtSe_2$ flake using regular Hall bar devices with constant dc bias current of 10 μA and magnetic field applied perpendicular to the flake.

X-ray photoemission spectroscopy. The experiments were performed in a spectrometer chamber equipped with a SPECS PHOIBOS150 hemispherical energy analyzer and a monochromatic SPECS XR-MF X-ray source (Al $K = 1486.7$ eV). The X-ray source was operated at 100 W, and the energy analyzer was set with 40 eV pass energy.

Data availability

Materials and data that support the findings of this research are available within the paper. All data are available from the corresponding author upon request.

Received: 10 January 2020; Accepted: 27 April 2020;
Published online: 25 May 2020

References

1. Wan, X., Turner, A. M., Vishwanath, A. & Savrasov, S. Y. Topological semimetal and Fermi-arc surface states in the electronic structure of pyrochlore iridates. *Phys. Rev. B* **83**, 205101 (2011).
2. Lv, B. Q. et al. Experimental discovery of Weyl semimetal TaAs. *Phys. Rev. X* **5**, 031013 (2015).
3. Xu, S.-Y. et al. Discovery of a Weyl fermion semimetal and topological Fermi arcs. *Science* **349**, 613–617 (2015).
4. Armitage, N. P., Mele, E. J. & Vishwanath, A. Weyl and Dirac semimetals in three-dimensional solids. *Rev. Mod. Phys.* **90**, 015001 (2018).
5. Young, S. M. et al. Dirac semimetal in three dimensions. *Phys. Rev. Lett.* **108**, 140405 (2012).
6. Wang, Z. et al. Dirac semimetal and topological phase transitions in A_3Bi (A=Na, K, Rb). *Phys. Rev. B* **85**, 195320 (2012).
7. Yan, B. & Felser, C. Topological materials: Weyl semimetals. *Annu. Rev. Condens. Matter Phys.* **8**, 337–354 (2017).
8. Liu, Z. K. et al. Discovery of a three-dimensional topological Dirac semimetal, Na_3Bi. *Science* **343**, 864–867 (2014).
9. Borisenko, S. et al. Experimental realization of a three-dimensional Dirac semimetal. *Phys. Rev. Lett.* **113**, 027603 (2014).
10. Soluyanov, A. A. et al. Type-II Weyl semimetals. *Nature* **527**, 495 (2015).
11. Sun, Y., Wu, S.-C., Ali, M. N., Felser, C. & Yan, B. Prediction of Weyl semimetal in orthorhombic $MoTe_2$. *Phys. Rev. B* **92**, 161107 (2015).
12. Fei, F. et al. Nontrivial Berry phase and type-II Dirac transport in the layered material $PdTe_2$. *Phys. Rev. B* **96**, 041201 (2017).
13. Wu, Y. et al. Observation of Fermi arcs in the type-II Weyl semimetal candidate WTe_2. *Phys. Rev. B* **94**, 121113 (2016).
14. Deng, K. et al. Experimental observation of topological Fermi arcs in type-II Weyl semimetal $MoTe_2$. *Nat. Phys.* **12**, 1105–1110 (2016).
15. Tamai, A. et al. Fermi arcs and their topological character in the candidate type-II Weyl semimetal $MoTe_2$. *Phys. Rev. X* **6**, 031021 (2016).
16. Yan, M. et al. Lorentz-violating type-II Dirac fermions in transition metal dichalcogenide $PtTe_2$. *Nat. Commun.* **8**, 257 (2017).
17. Zhang, K. et al. Experimental evidence for type-II Dirac semimetal in $PtSe_2$. *Phys. Rev. B* **96**, 125102 (2017).
18. Noh, H.-J. et al. Experimental realization of type-II Dirac fermions in a $PdTe_2$ superconductor. *Phys. Rev. Lett.* **119**, 016401 (2017).
19. Nielsen, H. B. & Ninomiya, M. The Adler–Bell–Jackiw anomaly and Weyl fermions in a crystal. *Phys. Lett. B* **130**, 389–396 (1983).
20. Son, D. T. & Spivak, B. Z. Chiral anomaly and classical negative magnetoresistance of Weyl metals. *Phys. Rev. B* **88**, 104412 (2013).
21. Xiong, J. et al. Evidence for the chiral anomaly in the Dirac semimetal Na_3Bi. *Science* **350**, 413–416 (2015).
22. Zhang, C.-L. et al. Signatures of the Adler–Bell–Jackiw chiral anomaly in a Weyl fermion semimetal. Nature. *Nat. Commun.* **7**, 10735 (2016).
23. Li, H. et al. Negative magnetoresistance in Dirac semimetal Cd_3As_2. *Nat. Commun.* **7**, 10301 (2016).
24. Arnold, F. et al. Negative magnetoresistance without well-defined chirality in the Weyl semimetal TaP. *Nat. Commun.* **7**, 11615 (2016).
25. Yuan, Z., Lu, H., Liu, Y., Wang, J. & Jia, S. Large magnetoresistance in compensated semimetals $TaAs_2$ and $NbAs_2$. *Phys. Rev. B* **93**, 184405 (2016).
26. Liang, S. et al. Experimental tests of the chiral anomaly magnetoresistance in the Dirac–Weyl semimetals Na_3Bi and GdPtBi. *Phys. Rev. X* **8**, 031002 (2018).
27. Dai, X., Du, Z. Z. & Lu, H.-Z. Negative magnetoresistance without chiral anomaly in topological insulators. *Phys. Rev. Lett.* **119**, 166601 (2017).
28. Wang, Y. et al. Gate-tunable negative longitudinal magnetoresistance in the predicted type-II Weyl semimetal WTe_2. *Nat. Commun.* **7**, 13142 (2016).
29. Lv, Y.-Y. et al. Experimental observation of anisotropic Adler–Bell–Jackiw anomaly in type-II weyl semimetal WTe_2 crystals at the quasiclassical regime. *Phys. Rev. Lett.* **118**, 096603 (2017).
30. Li, P. et al. Evidence for topological type-II Weyl semimetal WTe_2. *Nat. Commun.* **8**, 2150 (2017).
31. Huang, H., Zhou, S. & Duan, W. Type-II Dirac fermions in the $PtSe_2$ class of transition metal dichalcogenides. *Phys. Rev. B* **94**, 121117 (2016).
32. Li, Z., Zeng, Y., Zhang, J., Zhou, M. & Wu, W. Observation of negative longitudinal magnetoresistance in the type-II Dirac semimetal $PtSe_2$. *Phys. Rev. B* **98**, 165441 (2018).
33. Yang, H. et al. Quantum oscillations in the type-II Dirac semi-metal candidate $PtSe_2$. *N. J. Phys.* **20**, 043008 (2018).
34. Liu, E. et al. Integrated digital inverters based on two-dimensional anisotropic ReS_2 field-effect transistors. *Nat. Commun.* **6**, 6991 (2015).
35. Ciarrocchi, A., Avsar, A., Ovchinnikov, D. & Kis, A. Thickness-modulated metal-to-semiconductor transformation in a transition metal dichalcogenide. *Nat. Commun.* **9**, 919 (2018).
36. Iwasaki, T. et al. Hydrogen intercalation: an approach to eliminate silicon dioxide substrate doping to graphene. *Appl. Phys. Express* **8**, 015101 (2014).
37. Burkov, A. A. Negative longitudinal magnetoresistance in Dirac and Weyl metals. *Phys. Rev. B* **91**, 245157 (2015).
38. Yu, Z.-M., Yao, Y. & Yang, S. A. Predicted unusual magnetoresponse in type-II Weyl semimetals. *Phys. Rev. Lett.* **117**, 077202 (2016).
39. Slager, R.-J., Juričić, V., Lahtinen, V. & Zaanen, J. Self-organized pseudo-graphene on grain boundaries in topological band insulators. *Phys. Rev. B* **93**, 245406 (2016).
40. Zhang, K., Zhang, E., Xia, M., Gao, P. & Zhang, S. The axial anomaly in chiral tilted Weyl semimetals. *Ann. Phys.* **394**, 1–16 (2018).

Acknowledgements

This work was supported by the National Natural Science Foundation of China (Grant No. 11804397) and Hunan High-level Talent Program (Grant No. 2019RS1006). Part of this work was supported by Grants-in-Aid for Scientific Research (Grant No. 16H02204), Grants-in-Aid for Scientific Research on Innovative Areas “Science of hybrid quantum systems” (Grant No.15H05867) from Japan Society for the Promotion of Science, and National Natural Science Foundation of China (Grant No. 11804396).

Author contributions

J.S. conceived the project. J.S. fabricated the devices, preformed the electrical measurements, and analyzed the data with the help from R.S.D. and Y.Y. H.X. and Y.G. measured and analyzed the X-ray photoemission spectroscopy. W.L. developed the theoretical model. J.S. wrote the manuscript with input from W.L. and R.S.D. K.I. and X.L. discussed the results and commented on the manuscript.

Competing interests

The authors declare no competing interests.

Additional information

Supplementary information is available for this paper at https://doi.org/10.1038/s42005-020-0357-8.

Correspondence and requests for materials should be addressed to J.S.

Reprints and permission information is available at http://www.nature.com/reprints

Publisher’s note Springer Nature remains neutral with regard to jurisdictional claims in published maps and institutional affiliations.